Soft Matter

RSC Publishing

PAPER

View Article Online
View Journal | View Issue

Lipid mediated packing of transmembrane helices – a dissipative particle dynamics study†

Cite this: *Soft Matter*, 2013, **9**, 2673

Ayelet Benjamini[a] and Berend Smit*[abc]

Interactions of transmembrane (TM) helices play a key role in many cell processes. The configuration and cross angle these helices adopt are traditionally attributed to specific residue interactions. We present a different approach, in which specific residues are disregarded, and the role of the membrane in TM helix packing is investigated. We introduce a coarse-grained model of TM helices and obtain their characteristic configurations in the membrane both as a single helix and as paired helices. Our analysis shows that hydrophobic mismatch has a substantial effect in determining not only the tilt angles of TM helices but also the cross angles between helix pairs, for a large range of hydrophobic mismatches. We discuss the origin of this effect as well as the deviations from the common trend. Additionally, we explore the effect of hydrophobic mismatch on the Potential of Mean Force (PMF) between TM helices and discuss the importance of helical geometry in forming crossed configurations. Our observations suggest that hydrophobic mismatch must be taken into account when analyzing configurations of TM helix pairs. Hydrophobic mismatch through its effect on helix tilt can explain many cross-angle distribution features, making the role of specific interactions in determining helix pair configurations less significant.

Received 20th September 2012
Accepted 21st December 2012

DOI: 10.1039/c2sm27165f

www.rsc.org/softmatter

1 Introduction

Association of TM α-helices is the basis of many cell processes. Among the membrane proteins (MPs) that require a helix-assembly to function are ion channels,[1] GPCR membrane receptors[2] and integrins.[3] To probe the complex association of many α-helices, the dimerization of two α-helices is typically used as a case study. Understanding the factors determining helix–helix packing has therefore been the aim of several studies.[4–12]

Most models developed to explain helix–helix packing rely on specific residue interactions between the helices.[8–12] These theories predict that specific residue interactions control the packing angle between the two α-helices in a TM helix pair. In most of these models the role of the membrane is limited to constraining the protein diffusion in the two-dimensional plane of the membrane. It is, however, well-known that the membrane plays an important role in determining the tilt of TM helices[13–19] and also in mediating the interactions between TM helices.[15,20–25] These phenomena are driven by the hydrophobic mismatch, which is defined as the difference between the hydrophobic length of a helix and the hydrophobic thickness of the membrane it is embedded in. It is reasonable to expect that the membrane, and hence the hydrophobic mismatch, also plays a role in the helix–helix packing.

Recently, we analyzed a large database of TM helices to show that the tilt angle of natural TM helices is also correlated with their hydrophobic mismatch.[26] By taking this correlation into account, we show that the cross-angle distribution of natural helices is statistically indistinguishable from that of non-interacting TM helices, whose tilt angle is determined by the hydrophobic mismatch. This suggests that the distribution of cross angles in TM helices can largely be explained by membrane-mediated interactions, irrespective of specific residue interactions.

Computer simulations may be used to validate the hypothesis that the cross-angle distribution of TM helices can be obtained even in the absence of specific residue interactions. Several computational methods enable modeling of membrane proteins.[27,28] Coarse-grained (CG) simulations, in which sets of atoms are grouped together to one bead, allow faster computation and have been used to probe biologically relevant time and length scales.[16,23,29,30] These models were shown to be successful in predicting bulk material properties[31] as well as in describing molecular level phenomena.[32–34]

In this paper we explore the effect of hydrophobic mismatch on the cross-angle distribution of simulated TM helices. We simulate a CG model of a TM α-helix that contains no specific

[a]Department of Chemistry, University of California in Berkeley, Berkeley, CA, USA. E-mail: berend-smit@berkeley.edu; Fax: +1 510 642 8063; Tel: +1 510 642 9275

[b]Department of Chemical and Biomolecular Engineering, University of California in Berkeley, Berkeley, CA, USA

[c]Materials Sciences Division, Lawrence Berkeley National Laboratory, Berkeley, CA, USA

† Electronic supplementary information (ESI) available. See DOI: 10.1039/c2sm27165f

residue information and explore its interactions under various hydrophobic mismatch conditions. In our previous work[26] we confined our simulations to match helices from the OPM (Orientations of Proteins in Membranes) database.[35] Here we expand our observations to the full range of hydrophobic mismatch pairs.

This paper is structured as follows. In Section 2 we introduce our CG model. In Section 3.1 we present simulation results for the tilt angle of a single TM helix, showing its correlation with hydrophobic mismatch. In Section 3.2 we present simulation results for the cross-angle distribution of paired TM helices. We show that this distribution also depends on the hydrophobic mismatch and introduce the reference cross-angle distribution; the distribution of non-interacting helices with a given tilt angle distribution. Section 3.3 discusses possible reasons for deviation from this reference distribution and the extent to which each reason is observed in our simulations. We further explore membrane-mediated effects in Section 3.4 where we present results for the potential of mean force between two helices and finally, in Section 3.5, we discuss a special case of super-positive mismatched helices. A detailed description of our simulation technique and specific sampling methods is described in Section 4. We provide concluding remarks and discuss the possible role of the membrane in the folding of MPs in Section 5.

2 Model

2.1 CG model

In this work, we model three system components: water, lipids, and TM α-helices using a CG representation of beads (see Fig. 1). Each bead represents a set of three non-hydrogen atoms, on average (*e.g.* carbon atoms/water molecules), that are bundled together. Four types of beads are considered: (i) a water like bead, (w), representing three water molecules; (ii) a hydrophilic bead, (h), used to model the lipid head group as well as the marginal part of the helix; (iii) a hydrophobic tail bead, (t), used to model the hydrophobic lipid tail; and (iv) a hydrophobic protein bead, (p), used to model the hydrophobic core of a TM helix. The lipid model used in this work was built to represent dimyristoylphosphatidylcholine (DMPC). It was previously shown to reproduce the phase diagram of a bilayer-forming lipid.[36] It includes a head group consisting of three (h) beads and two tails each containing five (t) beads. We therefore label the model $h_3(t_5)_2$ (see Fig. 1).

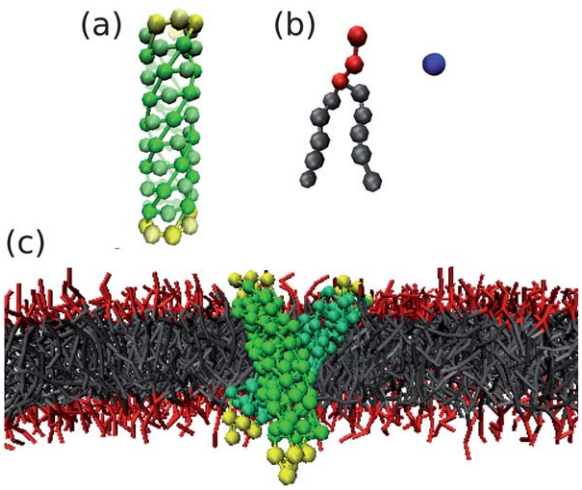

Fig. 1 Coarse-grained model. (a) CG model of an α-helix assembled from hydrophobic beads (green) and hydrophilic beads (yellow) at both ends to keep the helix transmembrane. (b) CG lipid model includes 3 hydrophilic head groups (red) and two 5-bead hydrophobic tails (grey). Water is represented explicitly by a single bead (blue). (c) shows a typical crossed configuration of two positive mismatched helices. Water particles are not displayed for clarity. All beads are of the same size and correspond to three non-hydrogen atoms.

This work extends previous publication by de Meyer *et al.*[23] Aside from the newly modeled α-helix, we use the same parameters for all system components. For a detailed description of lipid bonded interaction parameters, matrix of non-bonded interactions and DPD related parameters, see the work of de Meyer *et al.*

2.2 TM helix topology and interactions

Our transmembrane helix model contains three structural features: (i) N_p principal beads (P) that follow the outer radius structure of an α-helix backbone, represented in Fig. 1(a) by opaque beads. All structural bonds are associated with those beads. (ii) $N_s = N_p - 1$ secondary beads (S) located in between every adjacent pair of principal beads and provide the excluded volume along the helix exterior. These are represented in Fig. 1(a) by transparent beads. (iii) $N_c = N_p/3$ central beads (C) located along the central axis of the helix and provide the excluded volume at the helix interior.

To build our TM helix model we use the geometric parameters of a typical α-helix, by positioning our beads at the outer core of the helix. This mimics the helical structure by focussing on the surface accessible for interaction with other helices. We use a typical outer radius of $R_h = 6$ Å.[37] The angle and height pitch between consecutive principal beads follow the typical α-helix parameters: $\Delta\eta = 100°$; $\Delta Z = 1.5$ Å.[38] To generate the positions of N_p principal helix beads we chose an initial angle η_0 at random. We then place the first bead of the helix at position $\vec{r}_0 = (R_h \times \cos(\eta_0), R_h \times \sin(\eta_0), 0)$. The position of each principal bead thereafter, $P_{i=1\ldots N_{p-1}}$, is subsequently determined by $\vec{r}_i = (R_h \times \cos(\eta_0 + \Delta\eta \cdot i), R_h \times \sin(\eta_0 + \Delta\eta \cdot i), \Delta Z \cdot i)$.

We next position the secondary beads in between each pair of adjacent principal beads such that for each bead, $S_{j=0\ldots N_{s-1}}$;

$$\vec{r}_j = \left(R_h \times \cos\left(\eta_0 + \Delta\eta \cdot \left(j + \frac{1}{2}\right)\right), \right.$$

$$\left. R_h \times \sin\left(\eta_0 + \Delta\eta \cdot \left(j + \frac{1}{2}\right)\right), \ \Delta Z \cdot \left(j + \frac{1}{2}\right)\right).$$

Lastly, the central beads are positioned along the main axis of the helix. A central bead's z-component is determined by the average position of the three principal beads it is adjacent to. This yields for each central bead $C_{k=0\ldots N_{c-1}}$; $\vec{r}_k = (0, 0, \Delta Z \cdot (3k + 1))$.

Helix bead types are assigned such that the core of the helix consists of hydrophobic (p) beads, and its edges are

hydrophilic (h) beads. This assignment ensures that both edges of the protein remain in the water or membrane head group phase thus preventing unphysical configurations such as a helix lying within the membrane perpendicular to the membrane normal. Each hydrophilic edge of the helix consists of: three principal beads, two secondary beads and one central bead.

We apply bonded interactions to stabilize the helical structure, as described by the following set of potential energy functions:

$$U_{\text{bond}}(r) = \frac{1}{2}K_{\text{b}}\left(r - r_{\text{eq}}\right)^2 \quad (1a)$$

$$U_{\text{angle}}(\varphi) = \frac{1}{2}K_{\text{a}}\left(\varphi - \varphi_{\text{eq}}\right)^2 \quad (1b)$$

$$U_{\text{dihedral}}(\chi) = \frac{1}{2}K_{\text{d}}\left[\cos(\chi) - \cos\left(\chi_{\text{eq}}\right)\right]^2 \quad (1c)$$

Harmonic bond forces, derived from U_{bond} (1a), describe the force used to control the inter-bead distance. These are applied between: (a) each principal bead P_i and its two adjacent secondary beads $S_{j=i-1,i}$ (b) each two adjacent central beads C_k and C_{k+1} (c) each central bead C_k and its three adjacent principal beads $P_{i=3k,3k+1,3k+2}$, and (d) between each principal bead P_i and its consecutive P_{i+4} thus mimicking α-helix hydrogen bonding.

Harmonic bond constants are globally assigned to $K_{\text{b}} = 100\ \varepsilon_0/{d_0}^2$ continuing our assignment of bonded interaction parameters in the lipid model (reduced units of energy (ε_0) and length (d_0) are defined in Section 4). Equilibrium distances are derived from the helical structure and can be found in Table S1 of the ESI.† Since the role of central beads is to provide the excluded volume and not constrain the structure, interactions coupling the central pole and the helical structure have a decreased force constant of $K_{\text{b}} = 20\ \varepsilon_0/{d_0}^2$. The equilibrium distance for this interaction changes based on the position of the principle bead, as described in Table S1.†

Harmonic angle forces, derived from U_{angle} (1b), are used to control the stiffness of the helical structure. These are applied between: (a) each three consecutive principal beads: (P_i, P_{i+1}, P_{i+2}) (b) each three principal beads surrounding a hydrogen bond: (P_i, P_{i+4}, P_{i+5}), and (c) each three consecutive central beads: (C_k, C_{k+1}, C_{k+2}).

Harmonic angle force constants are assigned to a large $K_{\text{a}} = 600\ \varepsilon_0/\text{rad}^2$ for angles between consecutive principal beads as those are the most important for maintaining the helical structure. Supporting angle contributions, such as angles around hydrogen bonds are assigned an intermediate value of $K_{\text{a}} = 100\ \varepsilon_0/\text{rad}^2$. Angles involving central beads, which should only have a minor contribution to structural stability, are assigned a small value of $K_{\text{a}} = 20\ \varepsilon_0/\text{rad}^2$. Values for φ_{eq} can be found in Table S1.†

Dihedral angle forces, derived from U_{dihedral} (1c), regulate distortions in the helix structure and prevent the helix from unfolding. Therefore, changes in the protein's secondary structure are not described by this model. Those dihedral forces are applied between all sets of consecutive principal beads: (P_i, P_{i+1}, P_{i+2}, P_{i+3}). Note that helix structure features are controlled almost exclusively by interactions of principal beads. Secondary and central beads are positioned to serve as an exclusive volume and are only weakly bonded to ensure that they stay in close proximity to the helical structure.

We have performed several test simulations using different parameters for the bond, angle and dihedral angles. At certain parameter sets the helix structure starts falling apart and does not stay true to its helical nature. In all other parameter sets explored, which maintain the helix structure stability, we see consistent results for the tilt and cross angle distributions, in response to varying the hydrophobic mismatch.

3 Results and discussion

3.1 Tilt angles

To understand the configuration of packed helices, one must first understand the configuration of a single TM helix embedded in a lipid bilayer. The tilt angle of a helix, θ, is an important characteristic of single helix configuration. It is defined as the angle between the helix major axis and the bilayer normal. We measured the tilt angle for each helix as a function of its hydrophobic mismatch, Δd. The hydrophobic mismatch is defined as the difference between the hydrophobic length of the helix, d_{H}, and the hydrophobic thickness of a membrane, d_{L}. Mean and standard deviation values of tilt angles are shown in Fig. 2(a). We observe three regimes in the

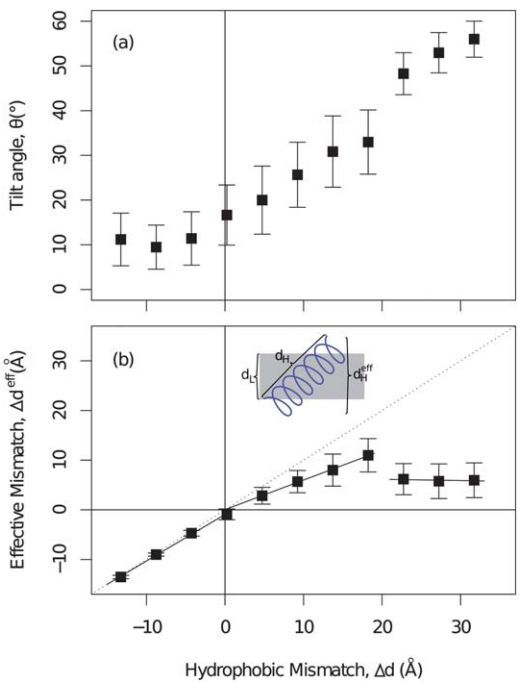

Fig. 2 Helix tilt angle (a) and effective hydrophobic mismatch (b) as a function of hydrophobic mismatch for single helices. We observe three regimes of hydrophobic mismatches. For $\Delta d < 0$ Å, the tilt angle plateaus and the effective hydrophobic mismatch matches the hydrophobic mismatch, with a slope of 0.94 (dashed line in (b) represents a slope of 1.0, for reference). For $\Delta d \in (0, 20]$ Å the tilt angle increases monotonically, and the slope of the effective mismatch decreases to 0.59; For $\Delta d > 20$ Å the effective mismatch stays constant at $\Delta d^{\text{eff}} \simeq 6$ Å while tilt angles increase. Solid lines in (b) represent linear fit of effective mismatch for each of the three regimes. Whiskers in both (a) and (b) represent one standard deviation.

behavior of tilt angles with respect to hydrophobic mismatch, which we refer to as: negative, positive, and super-positive mismatches.

For negative mismatched helices ($\Delta d < 0$ Å), we observe a plateau of $\langle\theta\rangle \sim 10^\circ$ in the tilt angle. This effect was previously observed for synthetic peptides,[14,16,19] though it differs significantly from what is observed in natural helices.[26] In synthetic helices, as well as in our current model, the ends of the helix are hydrophilic and so are forced to be in contact with the hydrophilic part of the membrane (or water). In those helices, tilting would decrease the effective hydrophobic size of the helix along the membrane normal, making it energetically unfavorable. The helix is therefore expected to tilt as little as entropically possible.[14] In natural helices, on the other hand, the ends of the helix are not necessarily hydrophilic, for such helices the tilt would be random.

For positive mismatched helices, $\Delta d \in (0, 20]$ Å, we observe an increase in the tilt angle of the helices as a function of hydrophobic mismatch. This increase matches with the previously reported results[14,16] and displays a slope similar to the one observed in natural helices.[26] In super-positive mismatched helices ($\Delta d \gtrsim 20$ Å) we observe a change in the slope of tilt angle, as helices tend to adopt a higher tilt angle. This effect has not been observed before as, to the best of our knowledge, this range of hydrophobic mismatches had not been explored previously. See Section 3.5 for further discussion on this regime.

The tilt of positive mismatched helices is the response of the system to decrease the hydrophobic mismatch. If a helix of hydrophobic size d_H adopts a non-zero tilt angle, θ, its effective hydrophobic length along the bilayer normal direction would decrease to $d_H^{eff} = d_H \cos(\theta)$, approaching the membrane hydrophobic thickness, d_L. We define the *effective hydrophobic mismatch* as the difference between the helix effective hydrophobic length and the bilayer hydrophobic thickness, $\Delta d^{eff} = d_H^{eff} - d_L = d_H \cos(\theta) - d_L$. It is a measure of the degree to which the hydrophobic mismatch strain is reduced by the tilting of a helix. If the helix was to tilt fully to match the membrane hydrophobic thickness, its effective mismatch would be $\Delta d^{eff} = 0$ Å, yielding a tilt angle of $\theta = \arccos(d_L/d_H)$.

The effective hydrophobic mismatch of our simulated TM helices is shown in Fig. 2(b). Again, we observe differences between the three major regimes. For negative-mismatched helices, the effective mismatch is nearly identical to the hydrophobic mismatch ($\Delta d^{eff} \propto 0.94\Delta d$). It is energetically unfavorable for these helices to decrease their hydrophobic length and so they preserve their length almost fully. Deviations from a slope of 1.0 originate in entropic contributions.

For positive-mismatched helices we observe a smaller slope, $\Delta d^{eff} \propto 0.59\Delta d$. In this range, there is an energetic balance between the adjustment of the helix, by tilting, and that of the membrane, by expanding its hydrophobic thickness around the helix (see Fig. S1 in the ESI†). We observe that the degree to which the helix reduces its hydrophobic size is fixed (60% of its mismatch) in the positive mismatch regime.

For super positive-mismatched helices, though, we observe a significant drop in the effective mismatch. Irrespective of the hydrophobic mismatch, the helices tilt to reach an effective mismatch of $\Delta d^{eff} \simeq 6$ Å. We observe a complimentary trend in the membrane thickness around super positive mismatched helices as well. The membrane thickness linearly increases with the hydrophobic mismatch of the embedded helix until it drops to a plateau for helices of super positive mismatch (see Fig. S1†). This suggests a shift in the balance of energetic contributions, and might point to a different arrangement of lipids around a super-positive mismatched helix. We discuss these results further in Section 3.5.

3.2 Crossed configurations

Traditionally, the cross angle of packed helices is thought to be determined by specific residue interactions. The fit between 'grooves' of one helix and the 'ridges' of its counter pair is believed to lock the packed configuration into the 'correct' cross angle. In our model, on the other hand, specific residues are not present as all beads are equivalent. This allows us to explore the role of the membrane in determining the cross-angle distribution in the absence of specific residue interactions.

Initially, we used the model of de Meyer *et al.*,[23] which represents peptides as cylinders with a hydrophobic core and two hydrophilic caps. For this model we found that the peptides tend to stay in a close-to-parallel configuration and do not form a cross. One could argue that in such a system a non-zero crossing angle can be obtained by electrostatic interactions. We therefore added partial charges along the surface of the cylinder, mimicking the presence of an α-helix dipole moment. Interestingly, adding these interactions did not induce a crossed configuration (see ESI and Fig. S2 for details†). The helical model, containing the same non-bonded interaction parameters but different geometry, however, did display configurations with a cross angle close to the experimentally observed angles (see Fig. S2†). These observations suggest that the helical geometry of beads is crucial for displaying a crossed configuration of TM peptides.

These observations present the following picture. The interface between two cylinders allows 'locking' of the beads in both cylinders. Since the surface of these cylinders is smooth, this locking mechanism is a cumulative sum of contributions from all beads along the surface. It therefore favors a parallel configuration where all beads can be 'locked', over a crossed configuration. In a helix, on the other hand, a similar 'locking' mechanism is hindered. The packing of beads in both helices is only apparent in a small part of the helix. The helices cannot, by geometric constraints, be locked to each other through more than a few residues, unless the helix flexes (as in coiled coils). We therefore hypothesize that the geometry of a helix, in contrast to a cylinder, supports the crossing of helices by *minimizing* the number of locked residues along the surface of the packed helices. In the remainder of this work we focus on the helical model.

We calculated the distribution of cross angle, (Ω), defined as the angle between the two helices major axes (see Section 4), for helix pairs. Our results show a relationship between the cross angle and hydrophobic mismatch. Cross-angle distributions of homogenous helix pairs are presented in Fig. 3. These show

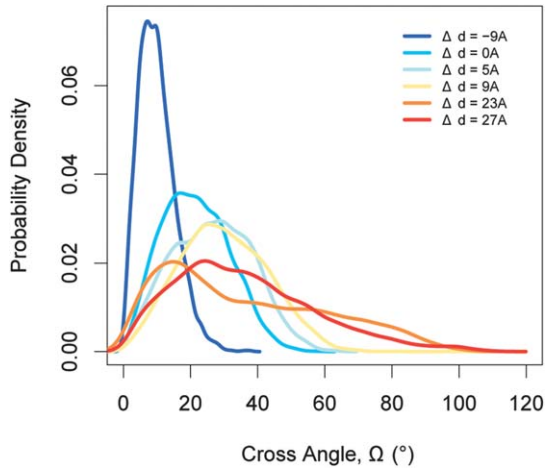

Fig. 3 Cross-angle distribution of homogeneous helix pairs. Each line represents the probability density of cross angles for one of six characteristic helix mismatches (see legend). Cross angles were collected only from packed configurations (inter-helical distance <15 Å).

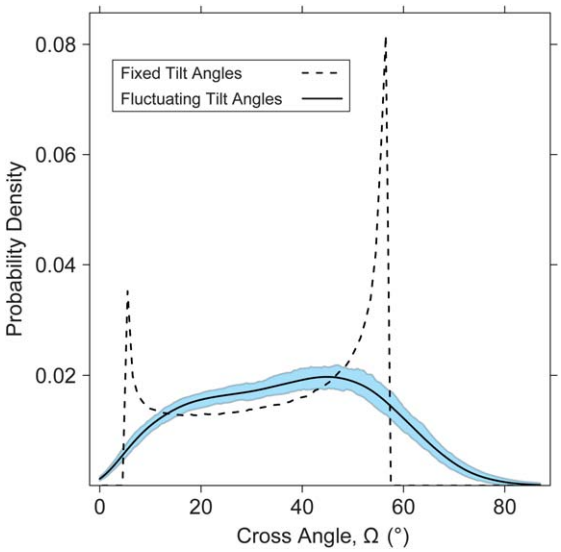

Fig. 4 Reference cross-angle distribution. Dashed line corresponds to the reference cross-angle distribution of two non-interacting helices with fixed tilt angles, θ'_1 and θ'_2, and random projection angle, γ; solid line corresponds to the reference cross-angle distribution of two helices with normally distributed tilt angles with mean θ'_1, θ'_2 and standard deviation σ_1, σ_2, respectively. These mean and standard deviation values correspond to the observed tilt angles for helices with hydrophobic mismatches $\Delta d_1 = 9$ Å, $\Delta d_2 = 14$ Å, respectively. These amount to $\theta'_1 = 25.7°$, $\theta'_2 = 30.8°$, $\sigma_1 = 5.9°$ and $\sigma_2 = 6.5°$. The shaded area around the reference distribution represents 90% confidence intervals.

clear dependence of the cross-angle distribution on the hydrophobic mismatch of helices. The mean cross angle value as well as the width of the distribution increases with increasing mismatch. This phenomenon was observed for natural helices[26] in experimental systems.

Benjamini and Smit[26] showed that the cross angle, Ω, and the helices tilt angle θ_1, θ_2 are not independent, even if the two helices do not interact with each other. Simple geometric consideration lead to the following relationship between the aforementioned angles along with γ, the projection angle (see angle definitions in Section 4.2):

$$\cos\Omega = \frac{(1+\cos\gamma)\cdot\cos(\theta_1-\theta_2)+(1-\cos\gamma)\cdot\cos(\theta_1+\theta_2)}{2} \quad (2)$$

This is a key relationship determining the cross angle of TM helix pairs. According to this relationship, for fixed tilt angles, θ'_1, θ'_2, the cross angle, Ω, would be confined to the range $|\theta'_1-\theta'_2| \le \Omega \le |\theta'_1+\theta'_2|$. The distribution of cross angles within that range would be non-uniform arcsine-like (see Fig. 4, dashed line).

TM helices do not have a fixed tilt angle, but rather a distribution of tilt angles. The overall cross-angle distribution of two such helices is therefore expected to be a weighted average of fixed tilt angle histograms. One such representative reference distribution is shown in Fig. 4 (solid line).

Based on the reference distribution, we expect the cross-angle distribution of two helices, even when far apart in the membrane, to display non-uniform distribution. Since the cross angle is confined by the sum and difference of the individual tilt angles, we expect the cross-angle distribution to be wider for helices with large tilt angles and less wide for helices with small tilt angles. Additionally, for pairs of helices with very different tilt angles ($\theta_1 \approx \theta_2$) we expect to see fewer small cross angles. Taking the correlation between hydrophobic mismatch and tilt into account, many characteristics of the distributions in Fig. 3 follow these expected behaviors. This suggests that the main dependence of the cross angle on the hydrophobic mismatch is through its effect on the tilt angles. We hypothesize that the hydrophobic mismatch controls the tilt of the individual helices, and that in turn confines the cross angle between those helices. This view matches our observations that the mean and spread of cross angles of homogeneous helix pairs grows with hydrophobic mismatch.

The effect of hydrophobic mismatch on the cross-angle distribution can be further observed in Fig. 5. Here we compared the cross-angle distribution of both homogenous and heterogenous pairs of helix mismatch with their reference distribution. The reference distribution for each helix pair was obtained by random sampling of tilt angles and projection angles. The resulting cross angle was calculated according to eqn (2). Tilt angles were sampled from a normal distribution, with the mean and standard deviation corresponding to the helix hydrophobic mismatch (as shown in Fig. 2(a)). Projection angles were sampled uniformly in the range [0°, 180°). The reference distribution is the distribution of cross angles for non-interacting helices, where each helix samples configurations as if it was alone in the membrane.

Fig. 5 shows a surprisingly good match between the simulation and reference cross-angle distribution. In both cases, reference and simulation, it is clear that the spread of the distribution, as well as the median cross angle, increases with mismatch. We define four groups of helix pairs, based on the hydrophobic mismatch of each of the paired helices (see Fig. 5 titles for group definitions). The agreement with the reference case is particularly good in the first two groups, I and II, of helix pairs which are both negative mismatched (or zero) and helix

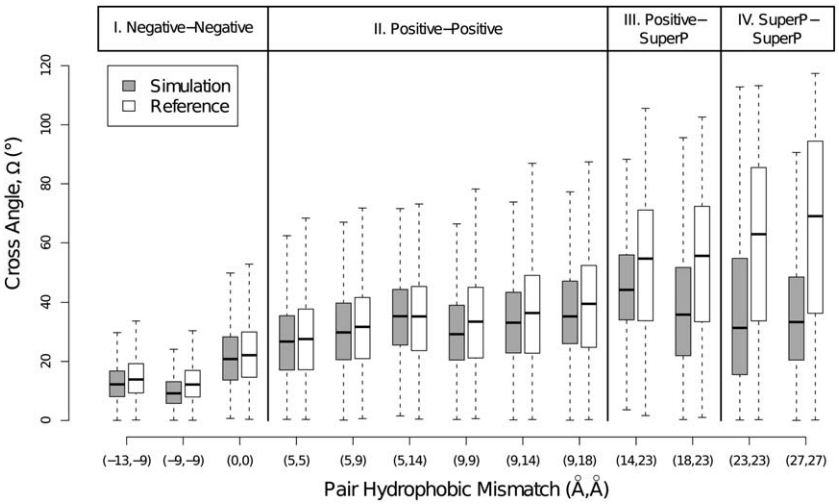

Fig. 5 Comparison of simulated cross-angle distributions (filled box-and-whisker diagrams) with their corresponding reference distributions (empty box-and-whisker diagrams). Each box represents the lower and upper quartiles around the median cross angle (horizontal black line). See ESI† for details on box-and-whisker representations. Simulated cross angles were collected only from packed configurations (inter-helical distance <15 Å). Helix pairs are segregated by vertical lines into four groups, depending on the mismatch of each helix in the pair, as represented in the group titles ('SuperP' refers to super-positive mismatched helices).

pairs which are both positive mismatched. The difference in the median cross angle (represented by the thick horizontal lines) from the reference distributions is on average only 2.3°. The spread of the simulated cross angles, as represented by the total height of the box, also seems to follow the same trend as the reference distribution, though it is consistently smaller in our simulated results (average 20% decrease). This effect is coupled with the bias in projection angles discussed in the next section. This particularly good agreement with reference distributions in the majority of helices (negative and positive mismatched) suggests the following. As the tilt angle is a dominant factor in determining the cross angle, and the tilt angle is set by the hydrophobic mismatch; in the majority of helices it is sufficient to understand the effect of hydrophobic mismatch on the individual tilt angles of the two helices, to obtain the effect on the cross-angle distribution.

For the latter groups (III and IV), containing super-positive mismatched helices, the agreement is not as good. The spread of the simulated distribution decreases by 33% on average compared to the reference distributions, and the difference in the median cross angle increases to 19.7°. This suggests a different response of the super-positive helices to the presence of another helix. We discuss this effect further in Section 3.5.

These effects, where the cross-angle distribution depends on the hydrophobic mismatch of individual helices, are not unique to simulated results. One can see evidence for that in natural TM helices as well.[26] This suggests a robust mechanism for determining the cross angle between TM helices. The hydrophobic mismatch of a helix in a membrane will determine to a large extent its relative orientation to other helices. Experimentally it has been observed that changes in the membrane thickness lead to changes in the protein structure and function.[39] While the cross angle of two helices is a very simplistic model for the protein structure, our observations show that changes in the membrane hydrophobic thickness can modulate the cross angle of packed helices. Combining these observations is a tempting suggestion, which we feel merits further studies.

3.3 Deviations from the reference distribution

The reference distribution of cross angles corresponds to a configuration of non-interacting, far-away helices. Deviations from the reference distribution are expected when helices are allowed to interact. In particular, three assumptions are made when constructing the reference distribution, and each can be invalidated for interacting helices: (a) projection angles are uniformly distributed between 0° and 180°; (b) tilt angles of both helices are uncorrelated; and (c) the distribution of helix tilt angles is equivalent to that of a single helix in the membrane. These assumptions are not independent, but the extent to which each one holds in a given pair can shed light on the way these helices interact. In this section we discuss the validity of each of these assumptions in simulated helix pairs. The results presented here refer only to packed configurations where the inter-helical distance is less than 15 Å.

3.3.1 Projection angle. For a pair of helices with fixed tilt angles, the projection angle, γ, is the independent variable determining the cross angle of the pair. *A priori*, there is no reason to expect one projection angle to be more favorable than others. The reference distribution of projection angles is therefore a uniform distribution: $\gamma \sim \mathcal{U}(0°,180°)$.

We compared the distribution of projected angles in simulated helix pairs to a reference uniform distribution in Fig. 6(a). The results vary based on the pair mismatch group. For a pair of two positive mismatched helices (group II), as well as for the zero-mismatched pair, we observe good agreement with the reference distribution, with a tendency towards marginally higher projection angles. The average median projection angle among this group is $\langle\gamma\rangle = 94.7° \pm 5.8°$ (compared to a reference

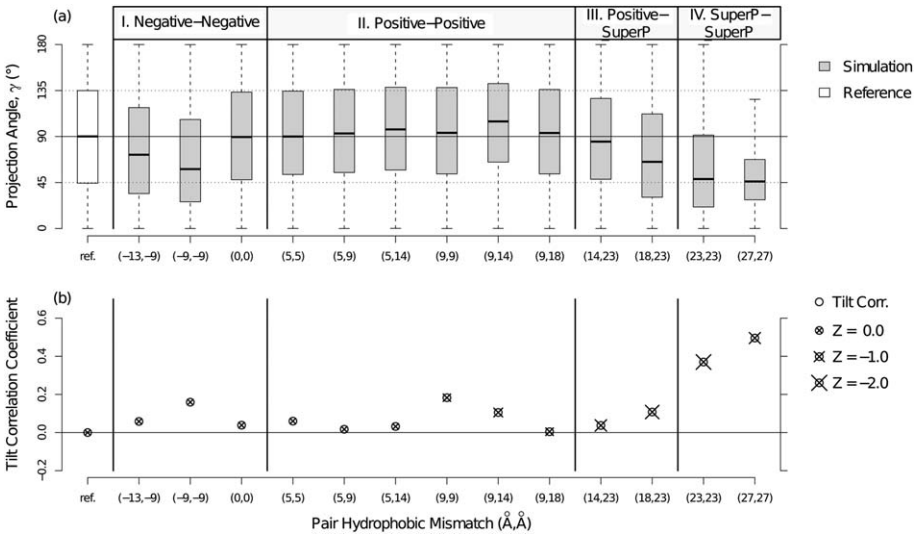

Fig. 6 Deviations from the reference distribution. (a) shows the distribution of projected angles. Simulated helix pairs are represented by grey filled box-and-whisker diagrams (details are provided in the ESI†). The white diagram represents the reference distribution of a uniform projection angle. Horizontal solid line corresponds to the mean projection angle of the reference distribution, $\gamma = 90.0°$; horizontal dotted lines correspond to the 25% and 75% percentiles of the reference distribution $\gamma = 90.0° \pm 45°$. (b) shows the tilt correlation and change in tilt distribution in helix pairs. Empty circles represent the correlation in the tilt angles between both helices in the simulated pair, with a standard error of 0.03. The size of the *x* symbol on each circle is proportional to the scaled mean distance (*Z*) of helix tilt angles, based on their distribution when isolated in the membrane (see legend and Table S2†). The bigger the symbol, the larger the difference is between the tilt angles of helices in a packed configuration compared to their individual tilt angle distributions. Group definitions are identical to those given in Fig. 5.

$\langle\gamma\rangle = 90°$). For other helix pairs (groups I, III, IV), we observe the opposite trend. The projection angle is biased towards lower values, with a median projection angle of $\langle\gamma\rangle = 60.0° \pm 15.1°$. The spread of the distribution, measured here by the size of the box is similar in all groups and amounts to $\langle\Delta\gamma\rangle = 80.8° \pm 4.5°$ (excluding the outlier (27 Å, 27 Å) pair). This value is somewhat smaller than that of the reference distribution ($\langle\Delta\gamma\rangle = 90°$).

One explanation for non-uniform projection angles and the tendency towards $\langle\gamma\rangle < 90°$ could originate from the frustration of lipid configurations. The number of lipids found between the ends of the two helices in a pair is directly proportional to γ. We show in Section 3.4, that the presence of a helix in the membrane is energetically unfavorable for the lipids. When confined by two helices, the lipids can be more constrained, which results in a driving force towards minimizing the number of lipids confined between the helices. A smaller projection angle decreases the number of lipids between helix ends. This might therefore explain the observed tendency towards lower projection angles.

3.3.2 Tilt correlation. Another means of measuring the deviation from the reference, non-interacting case is by comparing the tilt angles of the two helices in a pair. The non-interacting case assumes that the tilt angles of both helices are independent, with a correlation coefficient of 0. We calculated the correlation of tilt angles throughout the simulation and present the results in Fig. 6(b) (open circles). For groups I–III the correlation coefficient is smaller than 0.2, with an average of 0.07, suggesting no significant correlation between the tilt of both helices. For group IV, containing pairs of helices which are both super-positive mismatched, the correlation is much larger, reaching 0.37 ± 0.15 for the pair (23 Å, 23 Å) and 0.50 ± 0.22 for the pair (27 Å, 27 Å). This suggests cooperative tilting for pairs of super positive mismatched helices.

Another interesting observation relates to the average correlation coefficient in all pairs considered. Although in theory the full range of tilt correlation $[-1.0, 1.0]$ is accessible, in practice, the average correlation was positive in all pairs considered. Even though the average correlation in group I–III was rather small, the overall effect of having only positive correlation coefficient suggests somewhat cooperative tilting of all helices. Namely, if one helix tilted to a greater extent than its average tilt angle, so did the other helix, and *vice versa*.

3.3.3 Tilt distribution. When calculating the reference distribution we assume each helix samples tilt angles based on its single-helix distribution. This distribution corresponds to results presented in Fig. 2(a) where each helix is simulated alone in the membrane. In practice, the average tilt angles observed for each helix in a packed configuration are always *smaller* than their respective single-helix distribution. Detailed values are presented in Table S2 of the ESI.†

We calculate the differences in the distribution of tilt angles in paired *versus* single helix configuration, by determining the scaled mean distance (*Z*) for each helix pair (see details in the ESI†). A value of $Z = 0$ means that the distribution of tilt angles in the paired configuration is identical to the single-helix distribution. The larger the absolute value of *Z*, the larger the difference between these distributions. The results are presented by the *x* symbols in Fig. 6(b). These results show small differences in tilt angles for groups I–II, with an average *Z*-score of -0.25 (in units of standard deviation). This suggests that although tilt angles are smaller, the deviation from the single-helix histogram is not very large. For helix pairs with super-positive mismatched

helices the deviation from the single-helix distribution is much larger. The average *Z*-score in groups III–IV comes out to be −1.5 (in units of standard deviation).

The observations on tilt correlation (Section 3.3.2) and changes in tilt angle distribution when helices are paired (Section 3.3.3) present the following picture. The helices are by-and-large independently tilting, with a small tendency towards cooperative tilting. This results in an overall small but positive tilt correlation coefficient throughout all simulations. The presence of another helix shields some of the constraint originating in the hydrophobic mismatch, causing the helices to tilt less than when isolated in the membrane. When super-positive helices are present, the proposed shielding is enhanced, and both helices tilt significantly less than their respective single helix distribution. If two super-positive helices are in a packed configuration, the change in helix tilt becomes noticeably more cooperative. Combining these findings with the tendency towards small projection angles (Section 3.3.1) suggests that group IV helices adopt a tight, closer to parallel configuration where they behave as a single larger peptide and tilt together.

3.4 Potential of mean force

We calculate the potential of mean force (PMF) between pairs of TM helices as a function of the inter-helical distance (see details in the ESI†). The results depend greatly on the mismatch of the two helices in the pair, as shown in Fig. 7. For negative mismatched helices (Fig. 7(a)), we observe a short-range attraction followed by an intermediate-range repulsion. The strength of attraction, as well as the size of the barrier in intermediate distances, decreases with increasing mismatch (decreasing absolute mismatch). When the two helices are zero-mismatched the barrier diminishes and we observe only a very shallow ($\sim$0.6 k_BT) attraction well.

In positive mismatched helices we observe the reverse trend (Fig. 7(b)). The depth of the attractive well increases with growing mismatch. This can be viewed as the same effect as in negative mismatched helices, with respect to growing further from zero mismatch. Namely, the strength of attraction grows with the absolute value of the mismatch. The barrier in intermediated distances, however, is noticeably smaller for positive mismatched helices reaching a shear $\sim$0.6 k_BT. Additionally, the width of the attractive wells is wider for positive mismatched pairs, crossing the 0.0 potential line only at $r_0 \sim 33$ Å for the pair (9 Å, 9 Å) compared to a smaller $r_0 \sim 28$ Å for the pair (−9 Å, −9 Å).

Previous theoretical and simulation studies[23,40–42] showed that the range of attraction between TM proteins is fairly large, extending over several layers of lipid solvation shells, followed by an intermediate range repulsion. This characteristic potential profile originates from the line-tension forces of the liquid medium (lipid bilayer). Namely, the presence of proteins perturbs the membrane and creates a curved thickness profile. If the proteins are fairly close, it will be favorable to bring them together than to have two centers of perturbation. We see evidence for this behavior in our model as well. The fact that the attraction strength increases with the absolute mismatch, corresponding to larger deformation in the membrane thickness (Fig. S1†), enforces that hypothesis. If the helices are at intermediate (∼40 Å to 50 Å) distance from one another, the membrane thickness deformation at the intersection between the two helices has decreased. Bringing the helices closer together in this configuration will create larger line tension and would therefore be unfavorable, resulting in a potential barrier. At large distances the membrane thickness completely relaxes and so the helices do not feel each other's presence. We observe a plateau at the PMF in those ranges.

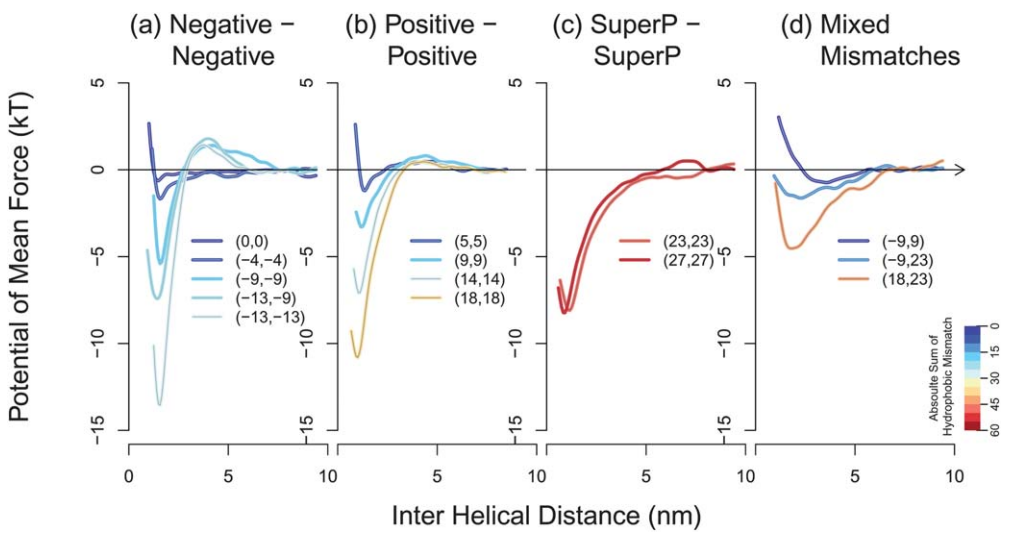

Fig. 7 Potential of mean force (PMF) between TM helices. Each line corresponds to a pair of helices. Mismatch values for both helices are provided in the legend in units of (Å, Å). Line colors correspond to the absolute sum of hydrophobic mismatch of both helices (see legend in bottom right corner). (a) shows the PMF of helix pairs who are both negative or zero mismatched; (b) both positive mismatched; (c) both super-positive mismatched, and (d) pairs of mixed mismatch groups. See Fig. S5 in the ESI† for detailed error bars.

The potential of mean force for super-positive mismatched helices is shown in Fig. 7(c). The strength of attraction for these helices does not grow with the mismatch, and is smaller than for the largest positive mismatched pair considered ((18 Å and 18 Å)). This observation fits the assumption that the potential of mean force between TM helices is greatly determined by the membrane thickness. As we show in Fig. S1,† the membrane thickness at $r = 0$ distance from the helix decreases and plateaus for super-positive mismatched helices. It is therefore expected that the strength of attraction between a pair of such helices will be smaller than that of positive mismatched helices.

In the last group considered, heterogenous pairs of TM helices (Fig. 7(d)), we observe a wide and shallow attractive well. In all three cases examined the depth of the attractive well is smaller than that of the corresponding homogenous pairs. This suggests that TM helices tend to associate with helices of similar mismatch. If the helices were of different mismatch, causing different deformations to the bilayer, there would still be a driving force to localize this disturbance. But, if the deformations were different in nature (negative mismatched helix with positive or super-positive mismatched helix, for example), the attraction would not be very large, reaching at most $-1.6\ k_BT$ for the pair (−9 Å, 23 Å).

3.5 Super-mismatched helices

The results presented in previous sections imply the existence of a special class of helices, super-positive mismatched. Though rare, some natural TM helices with hydrophobic mismatch greater than 19 Å can be found (to be precise, 21 TM helices out of the currently resolved structures, see Table S3 in the ESI†). Additionally, understanding the driving forces that control the configurations of super-positive mismatched helices can shed light on the forces acting on regular positive mismatched helices. It is therefore important to understand the characteristics of this class of helices.

For super-positive mismatched helices we observe a breakdown of the trend between the mismatch and tilt angle. It seems that when helices reach that large of a mismatch, the balance between the membrane and the helix energetics is disrupted. It becomes more favorable for the helix to tilt to a greater extent (Fig. 2(a)), while the membrane thickness drops to a smaller value, closer to the bulk thickness (Fig. S1†). The picture that emerges from our simulation analysis is presented in Fig. 8. For positive mismatched helices (Fig. 8(a) and (c)), the lipids accommodate the tilting helix by shielding its hydrophobic core from both top and bottom leaflets. This creates a frustrated lipid configuration as the density of lipid tails and heads deviate from its bulk value. As the helix grows larger so does its tilt angle, and the lipids on both leaflets get further frustrated. When the helix reaches a certain mismatch, it becomes more favorable for the helix to tilt to a greater degree, while the lipids shield it only from one leaflet. Namely, the face of the super-positive mismatched helix pointing 'down' ($-\hat{z}$) would be mostly shielded by lipids from the bottom leaflet; the face of the helix pointing 'up' ($+\hat{z}$) would be mostly shielded by lipids from the top leaflet. This alleviates the tension between lipid heads and tails.

Super-positive mismatched helices also tend to display a small projection angle and a large correlation of tilt angles when paired with other helices. This indicates a tendency towards tighter configurations, where the helices are bundled together to form one larger peptide.

These phenomena imply an entropic origin. We hypothesize the following scenario. For super-positive mismatched helices, representing a large volume exclusion, it is more favorable for the lipids to minimize the volume of inclusion and maximize the volume available for the lipids. This is done by pushing super-positive mismatched helices closer together into a tight configuration. In positive mismatched helices, the balance is reversed. The entropy of the helices, represented by their ability to explore a larger range of configurations (and projection angles), is greater than that of the lipids. This results in a configuration of rather-freely moving helices displaying a large set of projection angles and rather frustrated lipids in the vicinity of the helix pair.

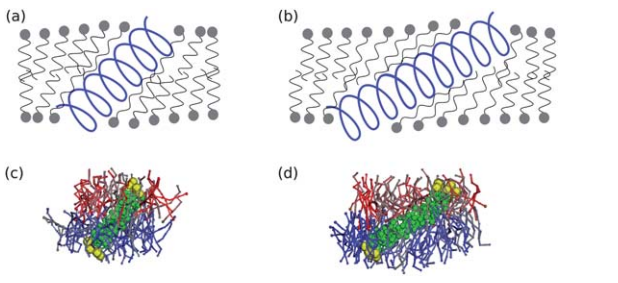

Fig. 8 Lipid configurations around positive mismatched ((a) and (c)) and super-positive mismatched ((b) and (d)) helices. (a) and (b) show a cartoon of lipid orientation around TM helices. (c) and (d) show snapshots from simulations of helices with mismatch $\Delta d = 13.73$ Å and 27.23 Å, respectively. Lower leaflet lipids are shaded blue and upper leaflet lipids are shaded red for clarity.

4 Methods

4.1 Simulation technique

We study the configurations of TM helices using a hybrid Dissipative Particle Dynamics-Monte Carlo (DPD-MC) simulation technique. In DPD,[43] a set of three forces combine together: a conservative force, $\vec{F}^C$, a dissipative force, $\vec{F}^D$, and a random force, $\vec{F}^R$. The conservative force includes all non-bonded interactions as well as bonded forces. The dissipative and random forces act together as a thermostat. The overall effect is a system simulated at constant temperature. The system equilibrium configurations are determined solely by the conservative (bonded and non-bonded) interactions.

To simulate the tensionless state of unconstrained lipid bilayers[44] we use Monte Carlo moves and sample from the $NP_\perp\gamma T$ ensemble. The bilayer surface tension, γ, is therefore set to be zero while the normal pressure, $P_\perp$, is set to equal the bulk water pressure ($P^* = 22.3$ in reduced units). For a detailed description of the simulation technique and parameters we refer to previously published work.[31]

Energy and length are measured in reduced units: $\varepsilon_0 = 1k_BT$, $d_0 = 6.46$ Å respectively. The cutoff radius for non-bonded

interactions is defined as $R_c \equiv 1d_0$. The temperature used throughout the simulations is $k_BT^* = 0.7\varepsilon_0$ in which the lipid bilayer is well within the L_α phase (~60 °C, see temperature scale in Venturoli *et al.*[45]).

The number of lipids was approximately 2000 lipids. Initially, we equilibrate a bilayer of 2024 lipids. We then make room for each helix (either one or two helices were simulated) by removing any lipids within the R_h (helix radius) distance from the point of helix insertion. To avoid unphysical biases in surface tension between the leaflets we remove an equal number of lipids from both bilayer leaflets. We then insert a helix of a given size into the bilayer (helix major axis parallel to bilayer normal). For a system with only a single helix, we simulate for 8×10^4 cycles, equivalent to ~100 ns. For a system of two helices we prepare 30 separate copies of the system, to gain a larger ensemble of configurations to sample from. We simulate each copy of the system for 2×10^4 cycles.

4.2 Sampling helix properties

In this work we sample various characteristics of the helix and the helical-dimer structure. For most properties investigated (*e.g.* cross angle and tilt angle) we use the helix major axis. To that end we find the center of mass of the four extreme principal beads at both ends of the helix. We then define the helix vector, $\vec{H}_i$, as the vector connecting those top and bottom end points (T_i and B_i, respectively) at each step in time for the i^{th} helix. We sample the helix radius as the average distance of each principal bead from the helix main vector. We ensure that the structure of the helix is robust by maintaining a constant average helix radius throughout the simulation.

Calculation of the distance between a pair of helices is done by using the Point of Closest Approach (PCA) algorithm following the procedure provided by Sunday.[46] In this method we first find a vector, $\vec{w}_c$, connecting the two helices lines: $\mathbf{L}_1(s) = B_1 + s\cdot\vec{H}_1$ and $\mathbf{L}_2(t) = B_2 + t\cdot\vec{H}_2$. As many such connecting vectors exist we chose the vector with the shortest size connecting the points of the helices that are in closest approach. Namely, we find the parameters (s_c, t_c) for which $|\vec{w}_c| = |\mathbf{L}_1(s_c) - \mathbf{L}_2(t_c)|$ is minimized. The distance between the helices is then defined as the size of the connecting vector, $r_{1,2} = |\vec{w}_c|$. We confine (s_c, t_c) to the range $0 \leq s_c, t_c \leq 1$, forcing the point of closest approach to be a physical point on each helix. This ensures the calculated distance is the closest physical distance between the helices.

Tilt angles for each TM helix, as well as the cross and projection angle for each helix pair were defined based on the helices major axes. The tilt angle, θ, was defined as the angle between the helix major axis and the normal to the bilayer, $+\hat{z}$. The helix major axis was always defined as pointing towards the $+\hat{z}$ direction, therefore limiting θ to the range [0°, 90°). The inter-helical cross angle, Ω, was defined as the 3D angle between the two helices major axes, $\Omega = \arccos(\vec{H}_1\cdot\vec{H}_2)$. It is limited to the range [0°, 180°). The inter-helical projection angle, γ, was defined as the 2D angle between the two helices major axes along the plane of the membrane ($\hat{x}$–$\hat{y}$). It is limited to the range [0°, 180°).

The hydrophobic mismatch of each helix was calculated based on the hydrophobic length of the helix and that of the membrane ($\Delta d = d_H - d_L$). Helix and membrane hydrophobic lengths were calculated as described in Benjamini and Smit.[26] We simulate 11 different helix sizes, with the number of principal beads corresponding to: $N_p = 15, 18, 21, 24, 27, 30, 33, 36, 39, 42, 45$. Their hydrophobic mismatch values correspond to: $\Delta d = -13.27$ Å, -8.77 Å, -4.27 Å, 0.23 Å, 4.73 Å, 9.23 Å, 13.73 Å, 18.23 Å, 22.73 Å, 27.23 Å, 31.72 Å, respectively.

5 Conclusions

In this work we explored the effect of hydrophobic mismatch on the cross-angle distribution, as well as other configurational parameters, of TM helices. We show that, even in the full range of hydrophobic mismatches, the cross-angle distribution of model TM helices is non-uniform and depends, both in mean and in spread, on the hydrophobic mismatch of helices. We additionally show that the cross-angle distribution of simulated helices matches to a great extent that of two non-interacting helices. Deviations from that distribution are hypothesized to result from membrane mediated forces pushing the helices towards the smaller projection angle, for example. Membrane mediate forces also induce association of TM helices.

These results have important implications on understanding the driving forces for helical packing. In our model, we do not define any specific residues. Yet we get a large deviation in cross-angle distribution when presented a different mismatch. This observation is in contrast to the current belief that specific residue interactions determine the cross angle. Our results suggest that when attributing a cross angle between helices to a specific residue interaction, one must account for all system components. Hydrophobic mismatch, through its effect on the tilt angle of both helices, might to a large extent explain the cross-angle distribution.

Acknowledgements

This work was supported by the Director, Office of Science, Office of Basic Energy Sciences, Division of Chemical, Geological and Biosciences of the U.S. Department of Energy under Contract no. DE-AC02-05CH11231.

References

1 W. N. Green and N. S. Millar, *Trends Neurosci.*, 1995, **18**, 280–287.
2 M. J. Lohse, *Curr. Opin. Pharmacol.*, 2010, **10**, 53–58.
3 D. Cox, M. Brennan and N. Moran, *Nat. Rev. Drug Discovery*, 2010, **9**, 804–820.
4 E. Psachoulia, D. P. Marshall and M. S. P. Sansom, *Acc. Chem. Res.*, 2010, **43**, 388–396.
5 F. Cymer and D. Schneider, *Cell Adhes. Migrat.*, 2010, **4**, 299–312.
6 E. Li and K. Hristova, *Cell Adhes. Migrat.*, 2010, **4**, 249–254.
7 J. Liang, *Curr. Opin. Chem. Biol.*, 2002, **6**, 878–884.

8 K. G. Fleming, A. L. Ackerman and D. M. Engelman, *J. Mol. Biol.*, 1997, **272**, 266–275.
9 K. R. MacKenzie, J. H. Prestegard and D. M. Engelman, *Science*, 1997, **276**, 131–133.
10 S. Kim, T. J. Jeon, A. Oberai, D. Yang, J. J. Schmidt and J. U. Bowie, *Proc. Natl. Acad. Sci. U. S. A.*, 2005, **102**, 14278–14283.
11 N. Sal-Man, D. Gerber, I. Bloch and Y. Shai, *J. Biol. Chem.*, 2007, **282**, 19753–19761.
12 R. F. S. Walters and W. F. DeGrado, *Proc. Natl. Acad. Sci. U. S. A.*, 2006, **103**, 13658–13663.
13 S. H. Park and S. J. Opella, *J. Mol. Biol.*, 2005, **350**, 310–318.
14 S. K. Kandasamy and R. G. Larson, *Biophys. J.*, 2006, **90**, 2326–2343.
15 J. Lee and W. Im, *J. Am. Chem. Soc.*, 2008, **130**, 6456–6462.
16 L. Monticelli, S. K. Kandasamy, X. Periole, R. G. Larson, D. P. Tieleman and S. J. Marrink, *J. Chem. Theory Comput.*, 2008, **4**, 819–834.
17 T. Kim and W. Im, *Biophys. J.*, 2010, **99**, 175–183.
18 A. Holt and J. A. Killian, *Eur. Biophys. J.*, 2010, **39**, 609–621.
19 E. Strandberg, S. Esteban-Martin, A. S. Ulrich and J. Salgado, *Biochim. Biophys. Acta, Biomembr.*, 2012, **1818**, 1242–1249.
20 J. A. Killian, I. Salemink, M. R. R. dePlanque, G. Lindblom, R. E. Koeppe and D. V. Greathouse, *Biochemistry*, 1996, **35**, 1037–1045.
21 J. H. Ren, S. Lew, J. Y. Wang and E. London, *Biochemistry*, 1999, **38**, 5905–5912.
22 E. Sparr, W. L. Ash, P. V. Nazarov, D. T. S. Rijkers, M. A. Hemminga, D. P. Tieleman and J. A. Killian, *J. Biol. Chem.*, 2005, **280**, 39324–39331.
23 F. J.-M. de Meyer, M. Venturoli and B. Smit, *Biophys. J.*, 2008, **95**, 1851–1865.
24 L. V. Schaefer, D. H. de Jong, A. Holt, A. J. Rzepiela, A. H. de Vries, B. Poolman, J. A. Killian and S. J. Marrink, *Proc. Natl. Acad. Sci. U. S. A.*, 2011, **108**, 1343–1348.
25 D. L. Parton, J. W. Klingelhoefer and M. S. P. Sansom, *Biophys. J.*, 2011, **101**, 691–699.
26 A. Benjamini and B. Smit, *Biophys. J.*, 2012, **103**, 1227–1235.
27 W. L. Ash, M. R. Zlomislic, E. O. Oloo and D. P. Tieleman, *Biochim. Biophys. Acta, Biomembr.*, 2004, **1666**, 158–189.
28 E. Lindahl and M. S. P. Sansom, *Curr. Opin. Struct. Biol.*, 2008, **18**, 425–431.
29 P. J. Bond, J. Holyoake, A. Ivetac, S. Khalid and M. S. P. Sansom, *J. Struct. Biol.*, 2007, **157**, 593–605.
30 S. J. Marrink, H. J. Risselada, S. Yefimov, D. P. Tieleman and A. H. de Vries, *J. Phys. Chem. B*, 2007, **111**, 7812–7824.
31 F. J. M. de Meyer, A. Benjamini, J. M. Rodgers, Y. Misteli and B. Smit, *J. Phys. Chem. B*, 2010, **114**, 10451–10461.
32 S. J. Marrink, A. H. de Vries and D. P. Tieleman, *Biochim. Biophys. Acta, Biomembr.*, 2009, **1788**, 149–168.
33 J. Wong-Ekkabut, S. Baoukina, W. Triampo, I. M. Tang, D. P. Tieleman and L. Monticelli, *Nat. Nanotechnol.*, 2008, **3**, 363–368.
34 J. Gumbart and K. Schulten, *Biochemistry*, 2007, **46**, 11147–11157.
35 M. A. Lomize, A. L. Lomize, I. D. Pogozheva and H. I. Mosberg, *Bioinformatics*, 2006, **22**, 623–625.
36 M. Kranenburg, M. Venturoli and B. Smit, *J. Phys. Chem. B*, 2003, **107**, 11491–11501.
37 C. O. Pabo and R. T. Sauer, *Annu. Rev. Biochem.*, 1984, **53**, 293–321.
38 C. Branden and J. Tooze, *Introduction to Protein Structure*, Garland Pub., New York, 1991, pp. xv, 302 p.
39 O. S. Andersen and R. E. Koeppe, in *Bilayer Thickness and Membrane Protein Function: An Energetic Perspective*, Annual Reviews, Palo Alto, 2007, vol. 36, pp. 107–130.
40 K. Bohinc, V. Kralj-Iglic and S. May, *J. Chem. Phys.*, 2003, **119**, 7435–7444.
41 S. May and A. Ben-Shaul, *Biophys. J.*, 1999, **76**, 751–767.
42 M. M. Sperotto and O. G. Mouritsen, *Eur. Biophys. J.*, 1991, **19**, 157–168.
43 R. D. Groot and P. B. Warren, *J. Chem. Phys.*, 1997, **107**, 4423–4435.
44 F. Jahnig, *Biophys. J.*, 1996, **71**, 1348–1349.
45 M. Venturoli, B. Smit and M. M. Sperotto, *Biophys. J.*, 2005, **88**, 1778–1798.
46 D. Sunday, *Distance between Lines and Segments with CPA*, http://www.softsurfer.com/Archive/algorithm_0106/algorithm_0106.htm.